Commun. Comput. Phys.
doi: 10.4208/cicp.OA-2016-0200

Vol. **22**, No. 4, pp. 1049-1068
October 2017

High Order Well-Balanced Weighted Compact Nonlinear Schemes for Shallow Water Equations

Zhen Gao[1] and Guanghui Hu[2,3,*]

[1] *School of Mathematical Sciences, Ocean University of China, Qingdao, China.*
[2] *Department of Mathematics, University of Macau, Macao SAR, China.*
[3] *UM Zhuhai Research Institute, Zhuhai, Guangdong, China.*

Received 10 November 2016; Accepted (in revised version) 20 March 2017

Abstract. In this study, a numerical framework of the high order well-balanced weighted compact nonlinear (WCN) schemes is proposed for the shallow water equations based on the work in [S. Zhang, S. Jiang, C.-W Shu, J. Comput. Phys. 227 (2008) 7294-7321]. We employ a special splitting technique for the source term proposed in [Y. Xing, C.-W Shu, J. Comput. Phys. 208 (2005) 206-227] to maintain the exact C-property, which can be proved theoretically. In the meantime, the genuine high order accuracy of the numerical scheme can be observed successfully, and small perturbation of the stationary state can be resolved and evolved well. In order to capture the strong discontinuities and large gradients, the fifth-order upwind weighted nonlinear interpolations together with the fourth/sixth order cell-centered compact scheme are used to construct different WCN schemes. In addition, the local characteristic projections are considered to further restrain the potential numerical oscillations. A variety of representative one- and two-dimensional examples are tested to demonstrate the good performance of the proposed schemes.

AMS subject classifications: 35L65, 35L67

Key words: Shallow water equations, C-property, weighted compact nonlinear scheme, source term.

1 Introduction

The shallow water equations are usually a system of hyperbolic conservation laws with additional source terms that describes geophysical flows, especially when the horizontal length scale is much greater than the vertical length scale. The equations play an important role in the modeling and simulation of free surface flows in rivers and coastal

*Corresponding author. *Email addresses:* zhengao@ouc.edu.cn (Z. Gao), garyhu@umac.mo (G. H. Hu)

 ©2017 Global-Science Press

https://doi.org/10.4208/cicp.OA-2016-0200 Published online by Cambridge University Press

areas, and can predict tides, storm surge levels and coastline changes from hurricanes and ocean currents [33].

The two-dimensional shallow water equations can be written as

$$\frac{\partial h}{\partial t}+\frac{\partial (hu)}{\partial x}+\frac{\partial (hv)}{\partial y}=0, \tag{1.1a}$$

$$\frac{\partial (hu)}{\partial t}+\frac{\partial (hu^2+\frac{1}{2}gh^2)}{\partial x}+\frac{\partial (huv)}{\partial y}=-ghb_x, \tag{1.1b}$$

$$\frac{\partial (hv)}{\partial t}+\frac{\partial (huv)}{\partial x}+\frac{\partial (hv^2+\frac{1}{2}gh^2)}{\partial y}=-ghb_y, \tag{1.1c}$$

where b is the vertical height of the bottom topography, from an arbitrary level of reference, h is the water depth above the bottom topography, (u,v) is the velocity vector, and $g=9.812$ is the gravitational constant. Due to the practical importance, this system has been theoretically and numerically studied for many years [6,11,12,16,17,21,30,32–34]. As we know, this system admits stationary solutions in which the nonzero flux gradients can be exactly balanced by the source terms in the steady state case. In other words, a good numerical scheme should be capable of preserving the stationary solution $h+b=constant$ and $(u,v)=(0,0)$. Therefore, Vukovic and Sopta [32] made an important modification on the classical weighted essentially non-oscillatory (WENO) scheme [14] and applied it to the shallow water equations for preserving the balance between the flux gradient and source terms. The scheme was verified for maintaining the exact conservation property (C-property) [2,31], when applied to a quiescent flow, where b is a smooth or non-smooth topography of the sea floor. Then the exact C-property was demonstrated in the one-dimensional sediment transport equations [5]. In [27], Robers et al. proved the balancing between the flux gradient and the source term. Xing and Shu [34] proposed the high order well-balanced WENO scheme, which maintained the exact C-property and achieved genuine high order accuracy for the general solutions of the shallow water equations. However, numerical experiments show that the classical WENO scheme is too dissipative for complex flow structures such as turbulence [15]. In [11,35,36], the well-balanced Runge-Kutta discontinuous Galerkin methods for the shallow water equations were also proposed respectively in the last decade. We refer to [33] and references therein for more detailed descriptions on the well-balanced schemes.

To increase the resolution and decrease the dissipation of the simulations, the well-balanced hybrid upwind-WENO [21] and compact-WENO [39] schemes were designed respectively in solving the shallow water equations. In the hybrid schemes, how to generate a high quality shock indicator for discontinuities in a complex flow is nontrivial. It is an active research area [10,26], but out of the scope of this paper. Moreover, based on the idea of WENO scheme, a class of weighted compact nonlinear (WCN) schemes were developed [8,9] which has better wave resolution and similar ability to capture discontinuities as the classical WENO scheme. Then it has been extended to the ninth order [22,25,37] which demonstrates the increasing resolutions with the increasing orders.

https://doi.org/10.4208/cicp.OA-2016-0200 Published online by Cambridge University Press

The WCN schemes also show suitable freestream and vortex preservation properties on a wavy grid [24]. In order to preserve the positivity of both density and pressure in the complex flow problems with severe discontinuities, the robust WCN schemes were proposed in [7,20,23] respectively. The corresponding robust WCN scheme was successfully employed to simulate the hydrogen/air detonation [23]. To the best knowledge of the authors, there is rare work on the numerical study of the WCN schemes for the shallow water equations.

We are trying to fill the gap in this paper by introducing a numerical framework of the high order well-balanced WCN schemes for the one- and two-dimensional shallow water equations. With the help of a special splitting of the source term proposed in [34], the proposed numerical schemes can exactly maintain the steady state solution, which is analyzed in detail in the paper. Our numerical framework is an extension of the high order WCN scheme in [37]. We use the first order global Lax-Friedrichs flux splitting to introduce correct upwinding and enhance the numerical stability. To reach the high order accuracy, the fifth-order upwind weighted nonlinear interpolations together with the fourth/sixth order cell-centered compact schemes are employed. To further restrain the numerical oscillations around the strong discontinuities and large gradients, the local characteristic projections on the conservative fluxes are also considered. Besides the high order numerical accuracy and the non-oscillatory behavior, the ability on well resolving small perturbations of the proposed schemes can also be observed successfully from the numerical experiments. It is worth mentioning that, the extension of our framework to higher order cases is straightforward.

The paper is organized as follows. In Section 2, a brief review of the formulation of the high order WCN schemes is delivered. In Section 3, the high order well-balanced WCN schemes proposed for the shallow water equations is described in detail. In Section 4, the exact C-property, high order numerical accuracy, as well as the non-oscillatory property of the proposed numerical schemes are tested by a variety of benchmark examples. Conclusions are given in Section 5.

2 A review of weighted compact nonlinear scheme

Consider a uniformly spaced grid defined by the points $x_i = i\Delta x, i = 0,\cdots,N$, which are called cell centers, with cell boundaries given by $x_{i+\frac{1}{2}} = x_i + \frac{\Delta x}{2}$, where Δx is the uniform grid spacing. The semi-discretized form of (1.1) without source terms is transformed into the system of ordinary differential equations and solved by the method of lines

$$\frac{du_i(t)}{dt} = -f_i', \quad i = 0,\cdots,N, \tag{2.1}$$

where f_i' is the numerical approximation to the spatial derivative at the cell centers x_i.

https://doi.org/10.4208/cicp.OA-2016-0200 Published online by Cambridge University Press

2.1 Cell-centered compact scheme

Given the function values on a set of nodes, a linear cell-centered compact scheme [18] approximation to $f_i^{'}$ is expressed as

$$\beta f_{i-2}^{'}+\alpha f_{i-1}^{'}+f_i^{'}+\alpha f_{i+1}^{'}+\beta f_{i+2}^{'}=c\frac{f_{i+\frac{5}{2}}-f_{i-\frac{5}{2}}}{5\Delta x}+b\frac{f_{i+\frac{3}{2}}-f_{i-\frac{3}{2}}}{3\Delta x}+a\frac{f_{i+\frac{1}{2}}-f_{i-\frac{1}{2}}}{\Delta x}. \tag{2.2}$$

If $\beta=0$, $c=0$, a fourth $(\alpha=1/22)$ or sixth $(\alpha=9/62)$ order tridiagonal compact scheme can be obtained with $a=3(3-2\alpha)/8$ and $b=(22\alpha-1)/8$. The derivatives at the two boundary points f_0' and f_N' are computed by the fifth order WENO-Z scheme [3, 4] with the well-balanced technique [34].

2.2 The fifth-order weighted interpolation

Here, we briefly review the basic idea of the high order weighted nonlinear interpolation and take fifth order $(r=3)$ interpolation for example.

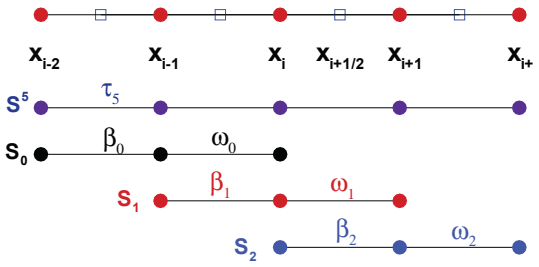


Figure 1: The uniformly spaced grid x_i and the 5-point stencil S^5, composed of three 3-point substencils $\{S_0,S_1,S_2\}$, used for the fifth-order weighted interpolation.

Similar to the idea of WENO reconstruction, the key issue of the weighted interpolation is the following polynomial reconstruction procedure. As shown in Fig. 1, the 5-point $(2r-1=5)$ global stencil S^5 is subdivided into three 3-point substencils $\{S_0,S_1,S_2\}$. The fifth degree polynomial approximation $\hat{f}_{i+\frac{1}{2}}=\tilde{f}(f_{i-2},\cdots,f_{i+2})$ is built through the convex combination of three second order interpolation polynomials $\hat{f}^k(x)$ in substencils $S_k, k=0,1,2$ at the cell boundaries $x_{i+\frac{1}{2}}$,

$$\begin{aligned}\hat{f}_{i+\frac{1}{2}}&=\frac{1}{128}(3f_{i-2}-20f_{i-1}+90f_i+60f_{i+1}-5f_{i+2})\\&=\sum_{k=0}^{2}C_k\hat{f}^k(x_{i+\frac{1}{2}}),\end{aligned} \tag{2.3}$$

https://doi.org/10.4208/cicp.OA-2016-0200 Published online by Cambridge University Press

where $(C_0,C_1,C_2)=(1/16,10/16,5/16)$ are the linear optimal weights and

$$\begin{aligned}\hat{f}^0(x_{i+\frac{1}{2}})&=\frac{1}{8}(3f_{i-2}-10f_{i-1}+15f_i),\\ \hat{f}^1(x_{i+\frac{1}{2}})&=\frac{1}{8}(-f_{i-1}+6f_i+3f_{i+1}),\\ \hat{f}^2(x_{i+\frac{1}{2}})&=\frac{1}{8}(3f_i+6f_{i+1}-f_{i+2}).\end{aligned}\tag{2.4}$$

To capture the discontinuities and high gradients without spurious oscillation, the idea of normalized nonlinear weights ω_k in the WENO reconstruction is used to replace the linear weights C_k. And then we can obtain the weighted interpolation approximation as [37]

$$\hat{f}_{i+\frac{1}{2}}=\sum_{k=0}^{2}\omega_k\hat{f}^k(x_{i+\frac{1}{2}}),\tag{2.5}$$

where

$$\omega_k=\frac{\alpha_k}{\sum_{j=0}^{2}\alpha_j},\quad \alpha_k=\frac{d_k}{(\beta_k+\varepsilon)^p},\quad k=0,1,2.\tag{2.6}$$

Here, the sensitivity parameter $\varepsilon>0$ is used to prevent the denominator from zero. The power parameter $p\geq 1$ is used to enhance the relative ratio among the smoothness indicators β_k which is defined by

$$\beta_k=\sum_{l=1}^{2}\Delta x^{2l-1}\int_{x_{i-\frac{1}{2}}}^{x_{i+\frac{1}{2}}}\left(\frac{d^l}{dx^l}\hat{f}^k(x)\right)^2dx,\quad k=0,1,2.\tag{2.7}$$

The explicit expressions for the smoothness indicators β_k can be found in [14, 37]. The weighting formulation Eq. (2.6) in the classical reconstruction procedure of the WENO scheme [14] is too dissipative to hold the accuracy at the critical points. An improved nonlinear weights [3, 4] are defined as

$$\alpha_k=d_k\left(1+\left(\frac{\tau_5}{\beta_k+\epsilon}\right)^p\right),\quad \omega_k=\frac{\alpha_k}{\sum_{l=0}^{2}\alpha_l},\quad k=0,1,2,\tag{2.8}$$

where $\tau_5=|\beta_2-\beta_0|$. $\varepsilon=10^{-12}$ and $p=2$ are used in this study.

The upwinding flux splitting technique is used to enhance the numerical stability

$$f(Q)=f^+(Q)+f^-(Q),\tag{2.9}$$

where $df^+(Q)/dQ\geq 0$ and $df^+(Q)/dQ\leq 0$. One example is a simple global Lax-Friedrichs flux splitting

$$f^{\pm}(Q)=\frac{1}{2}(f(Q)\pm\alpha Q),\tag{2.10}$$

https://doi.org/10.4208/cicp.OA-2016-0200 Published online by Cambridge University Press

where $\alpha=\max_i|\lambda_i(Q)|$ with $\lambda_i(Q)$ being the i-th eigenvalue of the Jacobian matrix $f'(Q)$, and $f^{\pm}(Q)$ are positive and negative fluxes respectively. See [14,28] for more details.

The fourth order cell-centered compact scheme combined with the fifth order weighted interpolation results in a fourth order weighted compact scheme. The sixth order cell-centered compact scheme combined with the fifth order weighted interpolation results in a fifth order weighted compact scheme respectively. We refer to [37] for the general formulation of the higher order weighted compact nonlinear schemes.

3 Well-balanced weighted compact nonlinear scheme

We first introduce the well-balanced WCN scheme for the one-dimensional shallow water equations by using the same idea in [34]. To maintain the steady state solution

$$h+b=constant,\quad u=0, \tag{3.1}$$

the source term $-ghb_x$ is reformulated equivalently into a sum of two terms $(gb^2)_x/2-g(h+b)b_x$. The corresponding one-dimensional shallow water equations (1.1) become

$$Q_t+F(Q)_x=S_x^1+S_x^2, \tag{3.2}$$

where $Q=(h,hu)^T$, $F=(hu,hu^2+gh^2/2)^T$, $S_x^1=(0,(gb^2)_x/2)^T$, $S_x^2=(0,-g(h+b)b_x)^T$. The flux $F(Q)$ is split up into

$$F(Q)=F^+(Q)+F^-(Q), \tag{3.3}$$

which can be defined by

$$F(Q)^{\pm}=\frac{1}{2}\left[\begin{pmatrix} hu \\ hu^2+\frac{1}{2}gh^2 \end{pmatrix}\pm\alpha\begin{pmatrix} h \\ hu \end{pmatrix}\right]. \tag{3.4}$$

One can replace $\pm\alpha\begin{pmatrix} h \\ hu \end{pmatrix}$ in Eq. (3.4) with $\pm\alpha\begin{pmatrix} h+b \\ hu \end{pmatrix}$ to maintain the steady state solution. Therefore, the flux splitting in Eq. (3.4) becomes

$$F(Q)^{\pm}=\frac{1}{2}\left[\begin{pmatrix} hu \\ hu^2+\frac{1}{2}gh^2 \end{pmatrix}\pm\alpha\begin{pmatrix} h+b \\ hu \end{pmatrix}\right]. \tag{3.5}$$

Similar techniques are used in the literature [34,38]. We refer to $Q^*=(h+b,hu)^T$ for clarity in the following proof. Moreover, the two derivatives in the source terms are also split up into their positive and negative parts as

$$\begin{pmatrix} 0 \\ \frac{1}{2}gb^2 \end{pmatrix}_x=\frac{1}{2}\begin{pmatrix} 0 \\ \frac{1}{2}gb^2 \end{pmatrix}_x^+ +\frac{1}{2}\begin{pmatrix} 0 \\ \frac{1}{2}gb^2 \end{pmatrix}_x^-,\quad \begin{pmatrix} 0 \\ b \end{pmatrix}_x=\frac{1}{2}\begin{pmatrix} 0 \\ b \end{pmatrix}_x^+ +\frac{1}{2}\begin{pmatrix} 0 \\ b \end{pmatrix}_x^-. \tag{3.6}$$

https://doi.org/10.4208/cicp.OA-2016-0200 Published online by Cambridge University Press

Proposition 3.1. Weighted compact nonlinear schemes with a linear interpolation Eq. (2.3) for the shallow water equations (3.2) satisfying the steady state solution Eq. (3.1) can maintain the exact C-property.

Proof.

$$\hat{F}^+_{j+\frac{1}{2}}=\sum_{k=-2}^{2}d_kF^+_{j+k}=\sum_{k=-2}^{2}d_k\frac{1}{2}(F_{j+k}+\alpha Q^*_{j+k})=\frac{1}{2}\sum_{k=-2}^{2}d_kF_{j+k}+\frac{1}{2}\sum_{k=-2}^{2}d_k(\alpha Q^*_{j+k}). \tag{3.7}$$

Similarly, we can obtain $\hat{F}^-_{j+\frac{1}{2}}$ as follows

$$\hat{F}^-_{j+\frac{1}{2}}=\tfrac{1}{2}\sum_{k=-1}^{3}e_kF_{j+k}-\tfrac{1}{2}\sum_{k=-1}^{3}e_k(\alpha Q^*_{j+k}). \tag{3.8}$$

Due to the constant vector Q^* and $\sum_{k=-2}^{2}d_k=\sum_{k=-1}^{3}e_k=1$, it follows that

$$\begin{aligned}&\sum_{k=-2}^{2}d_k(\alpha Q^*_{j+k})=\alpha(h+b,hu),\\&\sum_{k=-1}^{3}e_k(\alpha Q^*_{j+k})=\alpha(h+b,hu),\end{aligned} \tag{3.9}$$

then

$$\hat{F}_{j+\frac{1}{2}}=\hat{F}^+_{j+\frac{1}{2}}+\hat{F}^-_{j+\frac{1}{2}}=\frac{1}{2}\sum_{k=-2}^{2}d_kF_{j+k}+\frac{1}{2}\sum_{k=-1}^{3}e_kF_{j+k}. \tag{3.10}$$

We take the fourth order compact scheme Eq. (2.2) for example. The right hand side is

$$a\frac{\hat{F}_{j+\frac{1}{2}}-\hat{F}_{j-\frac{1}{2}}}{\Delta x}=\frac{a}{2\Delta x}\left(\sum_{k=-2}^{2}d_kF_{j+k}+\sum_{k=-1}^{3}e_kF_{j+k}\right)-\frac{a}{2\Delta x}\left(\sum_{k=-3}^{1}f_kF_{j+k}+\sum_{k=-2}^{2}d_kF_{j+k}\right). \tag{3.11}$$

By using the same procedure to two terms S^1_x and S^2_x of Eq. (3.2) and $g(h+b)=constant$, we can obtain

$$a\frac{\hat{S}^i_{j+\frac{1}{2}}-\hat{S}^i_{j-\frac{1}{2}}}{\Delta x}=\frac{a}{2\Delta x}\left(\sum_{k=-2}^{2}d_kS^i_{j+k}+\sum_{k=-1}^{3}e_kS^i_{j+k}\right)-\frac{a}{2\Delta x}\left(\sum_{k=-3}^{1}f_kS^i_{j+k}+\sum_{k=-2}^{2}d_kS^i_{j+k}\right), \tag{3.12}$$

with $i=1,2$. Therefore,

$$\begin{aligned}&a\frac{\hat{F}_{j+\frac{1}{2}}-\hat{F}_{j-\frac{1}{2}}}{\Delta x}-a\frac{\hat{S}^2_{j+\frac{1}{2}}-\hat{S}^2_{j-\frac{1}{2}}}{\Delta x}-a\frac{\hat{S}^2_{j+\frac{1}{2}}-\hat{S}^2_{j-\frac{1}{2}}}{\Delta x}\\&=\frac{a}{2\Delta x}\left(\sum_{k=-2}^{2}d_k(F_{j+k}-S^1_{j+k}-S^2_{j+k})\right)+\frac{a}{2\Delta x}\left(\sum_{k=-1}^{3}e_k(F_{j+k}-S^1_{j+k}-S^2_{j+k})\right)\\&\quad-\frac{a}{2\Delta x}\left(\sum_{k=-3}^{1}f_k(F_{j+k}-S^1_{j+k}-S^2_{j+k})\right)-\frac{a}{2\Delta x}\left(\sum_{k=-2}^{2}d_k(F_{j+k}-S^1_{j+k}-S^2_{j+k})\right),\end{aligned} \tag{3.13}$$

https://doi.org/10.4208/cicp.OA-2016-0200 Published online by Cambridge University Press

where $\sum_{k=-3}^{1} f_k = 1$. The first element in the vector $F_{j+k} - S^1_{j+k} - S^2_{j+k}$ is zero and the second element is

$$\frac{1}{2}gh^2 - \frac{1}{2}gb^2 + g(h+b)b = \frac{1}{2}g(h+b)^2. \tag{3.14}$$

Eq. (3.13) becomes

$$a\frac{\hat{F}_{j+\frac{1}{2}} - \hat{F}_{j-\frac{1}{2}}}{\Delta x} - a\frac{\hat{S}^2_{j+\frac{1}{2}} - \hat{S}^2_{j-\frac{1}{2}}}{\Delta x} - a\frac{\hat{S}^2_{j+\frac{1}{2}} - \hat{S}^2_{j-\frac{1}{2}}}{\Delta x} = 0. \tag{3.15}$$

Therefore, we can obtain $(hu^2 + \frac{1}{2}gh^2)_x - (\frac{1}{2}gb^2)_x + g(h+b)b_x = 0$. By similar procedure, the extension to other higher order WCN schemes is straightforward. This finishes the proof. □

However, the high order WCN schemes described in Section 2 are nonlinear. The nonlinearity comes from the nonlinear weights, which in turn comes from the nonlinearity of the smooth indicators β_k measuring the regularity of the fluxes F^+ and F^-. To maintain the exact C-property and accuracy, we use the same nonlinear weights as computed from the term $(hu^2 + gh^2/2)_x$ to two terms $(gb^2/2)_x$ and b_x respectively. Therefore, the nonlinear interpolation formulation Eq. (2.5) becomes a *linear* interpolation formulation in some sense and satisfies Proposition 3.1.

In the case of the characteristic-wise WCN schemes, we project the positive and negative fluxes on the characteristic fields via the left eigenvectors, the high order WCN reconstruction step is applied to obtain the high order approximation at the cell boundaries using the surrounding cell-centered values, which are then projected back into the physical space via the right eigenvectors and added together to form a high order numerical flux at the cell-interfaces. Moreover, the same left and right eigenvectors are projected to two terms in Eq. (3.6). The same nonlinear interpolation weights computed from the characteristic variables are used to the corresponding variables of Eq. (3.6) after the characteristic projection. One can use the similar procedure in Proposition 3.1 to prove that the characteristic-wise WCN schemes with the flux splitting Eq. (3.5), and with the special handling of the source terms described above, maintain exactly the C-property. For clarity, we present the algorithm of the characteristic-wise WCN scheme in the following flowchart.

ALGORITHM 3.1 (The characteristic-wise WCN scheme)**.** Given the flow fields Q and boundary conditions at time t_n and the final time T,

- **Step 1.** Do the flux splitting Eq. (3.5) and Eq. ((3.6).
- **Step 2.** Project the $F(Q)^{\pm}$ in Eq. (3.5) on the characteristic fields via the left eigenvectors, the high order WCN reconstruction step is applied to obtain the high order approximation and the corresponding nonlinear weights are saved. And then project back into the physical space via the right eigenvectors and added together to form a high order numerical flux at the cell-interfaces. Repeat the same projection to positive

https://doi.org/10.4208/cicp.OA-2016-0200 Published online by Cambridge University Press

and negative parts in Eq. (3.6) and use the saved nonlinear weights to obtain the high order approximation of $\frac{1}{2}gb^2$ and b at the cell-interfaces.

- **Step 3.** Use Eq. (2.2) to compute the derivatives of flux $F(Q)$ and source terms $\frac{1}{2}gb^2$ and b respectively.
- **Step 4.** Use the third-order TVD Runge-Kutta scheme to update the time integration.
- **Step 5.** If $t_{n+1}<T$, go to **Step 1**.

Finally, we consider the two-dimensional shallow water equations (1.1). The source terms are again reformulated as

$$-ghb_x=\left(\frac{1}{2}gb^2\right)_x-g(h+b)b_x,\quad -ghb_y=\left(\frac{1}{2}gb^2\right)_y-g(h+b)b_y, \tag{3.16}$$

and the one-dimension procedure described above is followed in the x- and y-directions respectively. All results proved in the one-dimensional case, such as the high order accuracy and the exact C-property can be similarly proved in the two-dimensional case.

The resulting system of ordinary differential equations after spatial discretization is advanced in time via the third order TVD Runge-Kutta scheme [29]. The CFL condition is set to be CFL = 0.45. We shall refer to the well-balanced WCN scheme above as the WCN scheme in the following discussion.

4 Numerical results

In this section, we will demonstrate the performance of the WCN schemes for solving the one- and two-dimensional shallow water equations. Several classical examples are presented. For clarity, the variance of the WCN schemes will be denoted as the `WCN-OrderCharacteristic` scheme where `Order` is the 4 (fourth) or 6 (sixth) order, and `Characteristic` is C (conservative flux without the local characteristic decomposition) or D (conservative flux with the local characteristic decomposition). For example, the WCN-4C scheme denotes the well-balanced WCN scheme with the fourth order compact scheme and the fifth order nonlinear interpolation is implemented on the conservative flux without the local characteristic decomposition. We shall collectively refer to all the WCN schemes as the WCN schemes. The reference solution is computed by the well-balanced WENO scheme [34] with $N=3000$ cells by replacing the WENO-JS scheme [14] with the WENO-Z scheme [4].

4.1 The accuracy of WCN scheme

To show the accuracy of WCN schemes, we solve the following scalar wave equation

$$Q_t+Q_x=0, \tag{4.1}$$

https://doi.org/10.4208/cicp.OA-2016-0200 Published online by Cambridge University Press

with the initial condition $Q(0,x)=sin(\pi x)$. The computational domain is $x\in[-1,1]$ and final time is $t=1$.

L_2, L_∞ errors and numerical orders of accuracy for the WCN-4C and WCN-6C schemes are given in Table 1. Obviously, the WCN schemes reach the expected convergence order as those in [37].

Table 1: The accuracy test. L_2, L_∞ errors and numerical orders of accuracy for the WCN-4C and WCN-6C schemes.

Method	N	L_2 error	L_2 order	L_∞	L_∞ order
WCN-4C	10	5.02E-3		5.19E-3	
	20	1.80E-4	4.80	1.84E-4	4.82
	40	8.10E-6	4.47	8.20E-6	4.49
	80	4.31E-7	4.23	4.37E-7	4.23
	160	2.51E-8	4.10	2.54E-8	4.10
	320	1.53E-9	4.04	1.54E-9	4.04
WCN-6C	10	4.19E-3		4.30E-3	
	20	1.21E-4	5.11	1.22E-4	5.14
	40	3.69E-6	5.04	3.75E-6	5.02
	80	1.15E-7	5.00	1.16E-7	5.01
	160	3.57E-9	5.01	3.58E-9	5.02
	320	1.11E-10	5.01	1.11E-10	5.01

4.2 Test for the one-dimensional exact C-property

The exact C-property is the most fundamental and crucial property for a numerical scheme for solving Eq. (3.2). Thus we follow the classical experiment in [34] to verify that the WCN schemes can maintain the exact C-property. The smooth and discontinuous bottom topographies are chosen as

$$b_1(x)=5e^{-\frac{2}{5}(x-5)^2},\quad b_2(x)=\begin{cases}4, & \text{if}\quad 4\le x\le 8,\\ 0, & \text{otherwise.}\end{cases} \tag{4.2}$$

The initial condition are given by

$$h+b=10,\quad hu=0.$$

The computational domain is $x\in[0,10]$ and the final time is $t=0.5$. We solve the problem using the WCN schemes with $N=100$, 200 and 400 cells. Theoretically, the stationary solution should be always exactly maintained (C-property).

We use double precision to perform the computation and show the L_∞ errors for the water surface level $h+b$ and water discharge hu in Tables 2 and 3. It can be clearly seen that those WCN schemes behave slightly different, but the L_∞ errors for both the smooth

https://doi.org/10.4208/cicp.OA-2016-0200 Published online by Cambridge University Press

Table 2: The one-dimensional exact C-property test. L_∞ errors in the water surface level $h+b$ and water discharge hu as computed by the WCN schemes with the smooth bottom topographies $b_1(x)$.

N	100		200		400	
L_∞	$h+b$	hu	$h+b$	hu	$h+b$	hu
WCN-4C	1.1E-14	7.5E-14	1.1E-14	1.1E-13	1.6E-14	1.7E-13
WCN-6C	8.9E-15	7.7E-14	1.1E-14	8.9E-14	1.6E-14	2.0E-13
WCN-4D	8.9E-15	9.3E-14	1.2E-14	1.0E-13	1.6E-14	1.3E-13
WCN-6D	8.9E-15	8.4E-14	1.2E-14	1.4E-13	1.8E-14	1.5E-13

Table 3: The one-dimensional exact C-property test. L_∞ errors in the water surface level $h+b$ and water discharge hu as computed by the WCN schemes with the discontinuous bottom topographies $b_2(x)$.

N	100		200		400	
L_∞	$h+b$	hu	$h+b$	hu	$h+b$	hu
WCN-4C	8.9E-15	8.4E-14	1.2E-14	9.9E-14	1.8E-14	1.6E-13
WCN-6C	7.1E-15	6.7E-14	2.0E-14	1.4E-13	1.4E-14	1.3E-13
WCN-4D	1.2E-14	8.5E-14	3.0E-14	2.6E-13	1.6E-14	1.8E-13
WCN-6D	8.9E-15	7.1E-14	2.0E-14	2.1E-13	2.3E-14	1.6E-13

and discontinuous bottom topographies are at the level of round-off errors. Therefore, the WCN schemes can preserve the exact C-property.

4.3 A small perturbation of one-dimensional steady state water

In this section, we consider a quasi-stationary test case given in [19] to demonstrate the capability of the WCN schemes for computation on a rapidly varying flow over a smooth bottom, and the perturbation of a stationary state. The bottom topography consists of a hump

$$b(x)=\begin{cases} 0.25(\cos(10\pi(x-1.5))+1), & \text{if} \quad 1.4\le x\le 1.6,\\ 0, & \text{otherwise.}\end{cases} \tag{4.3}$$

The initial conditions are

$$h(x,0)=\begin{cases} 1-b(x)+\xi, & \text{if} \quad 1.1\le x\le 1.2,\\ 1-b(x), & \text{otherwise,}\end{cases} \qquad u(x,0)=0, \tag{4.4}$$

where ξ is a nonzero constant amplitude of the perturbation. $\xi=0.2$ and $\xi=0.001$ are used in this study. The computational domain is $x\in[0,2]$ and the final time is $t=0.2$.

According to the classical behavior of wave propagation, the small disturbance will generate two smaller waves propagating to the left and right at the characteristic speeds $\pm\sqrt{gh}$. Many numerical methods have difficulty in the calculations involving such small perturbations of the water surface [19]. We show the water surface level $h+b$ and water discharge hu as computed by the WCN schemes with $N=300$ cells at time $t=0.2$ in Fig. 2.

https://doi.org/10.4208/cicp.OA-2016-0200 Published online by Cambridge University Press

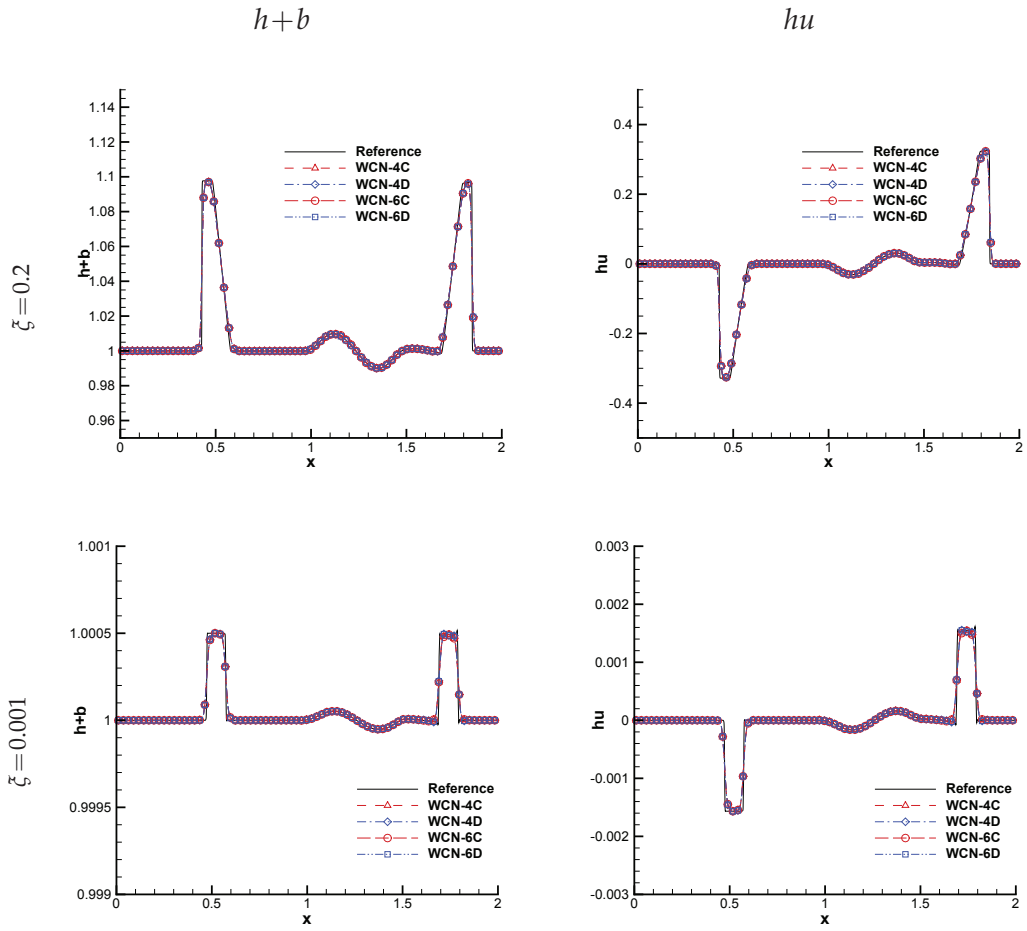


Figure 2: A small perturbation of one-dimensional steady state water with (Top) $\xi=0.2$ and (Bottom) $\xi=0.001$. (Left) The water surface level $h+b$ and (Right) water discharge hu as computed by the WCN schemes at time $t=0.2$.

The small traveling waves with an initial pulse perturbations are resolved accurately, free of spurious numerical oscillations. Furthermore, the results computed by the WCN schemes are overlapped and comparable to those given in the literature [19,34].

4.4 Discontinuous bottom topography

A discontinuous bottom topography in the form of Heaviside function [1] is given by

$$b(x)=\begin{cases} 0, & \text{if} \quad x\leq 0, \\ 1, & \text{otherwise.} \end{cases} \tag{4.5}$$

Two types of initial condition are as follows:

https://doi.org/10.4208/cicp.OA-2016-0200 Published online by Cambridge University Press

- 1-rarefaction and 2-shock problem:

$$h(x,0)=\begin{cases} 4, & \text{if} \quad x\leq 0, \\ 1, & \text{otherwise}, \end{cases} \qquad u(x,0)=0. \tag{4.6}$$

- 1-shock and 2-shock problem:

$$h(x,0)=\begin{cases} 4, & \text{if} \quad x\leq 0, \\ 1, & \text{otherwise}, \end{cases} \qquad u(x,0)=\begin{cases} 5, & \text{if} \quad x\leq 0, \\ -0.9, & \text{otherwise}. \end{cases} \tag{4.7}$$

The computational domain is $x\in[-10,10]$ and the final time is $t=1$.

A rarefaction wave propagating to the left and two shock waves traveling to the right with I.C. (4.6) and two shocks traveling in the opposite directions with I.C. (4.7) will be produced due to the nonlinear interaction of the discontinuous bottom topography and the system of nonlinear PDEs. The water surface level $h+b$ and its part of close-up view computed by the WCN schemes with 300 cells at time $t=1$ are shown in Fig. 3 which agree well with those in the literature [21]. From the zoomed figures, we can find that the WCN schemes without using the local characteristic decomposition (WCN-4C and WCN-6C) generate more numerical oscillations than other cases (WCN-4D and WCN-6D).

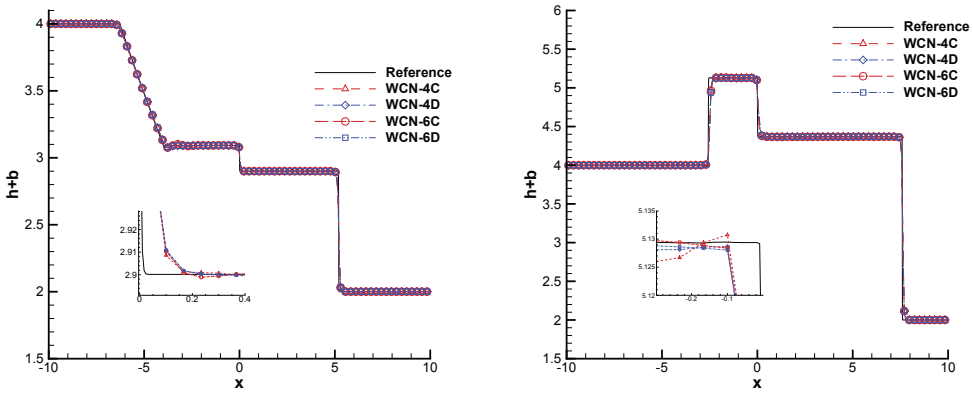


Figure 3: Discontinuous bottom topography. The water surface level $h+b$ of (Left) 1-rarefaction and 2-shock problem (Right) 1-shock and 2-shock problem as computed by the WCN schemes at time $t=1$.

4.5 One-dimensional dam-breaking problem over a rectangular bump

We choose a classical example in [32], that is the one-dimensional dam-breaking problem over a rectangular bump, to investigate the capability of the WCN schemes in the shock capturing under a more complex condition. It involves an unsteady flow over a

https://doi.org/10.4208/cicp.OA-2016-0200 Published online by Cambridge University Press

discontinuous bottom topography

$$b(x)=\begin{cases} 8, & \text{if} \quad |x-750|\leq 1500/8, \\ 0, & \text{otherwise.} \end{cases} \tag{4.8}$$

The initial conditions are

$$h(x,0)=\begin{cases} 20-b(x), & \text{if} \quad x\leq 750, \\ 15-b(x), & \text{otherwise,} \end{cases} \qquad u(x,0)=0. \tag{4.9}$$

The computational domain is $x\in[0,1500]$ and the final time is $t=60$.

The initial water surface level $h+b$ and the bottom topography b are drawn in the left figure of Fig. 4. The final water surface level $h+b$ computed by the WCN schemes with $N=500$ cells at the time $t=60$ is shown in the right figure of Fig. 4 which agrees well with those given in [34]. To demonstrate the good performance of the WCN schemes, we also show the water surface level $h+b$ and water discharge hu at time $t=15$ in Fig. 5 which is in a good agreement with the published results in [21,34]. Although the water depth h contains discontinuities at $x=562.5$ and $x=937.5$, the numerical solutions are essentially free of oscillations. However, from the zoom-in figures, the slightly numerical oscillations around the discontinuities can be observed in the cases of the WCN-4C and WCN-6C schemes.

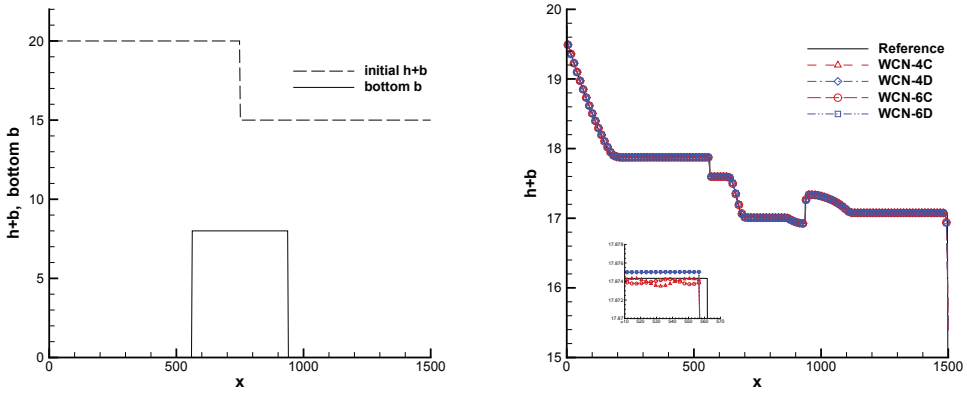


Figure 4: One-dimensional dam-breaking problem. (Left) The initial water surface level $h+b$ and the bottom topography b and (Right) the water surface level $h+b$ as computed by the WCN schemes at time $t=60$.

4.6 Test for the two-dimensional exact C-property

We follow the example in [34] to demonstrate that the two-dimensional exact C-property over a hump can be preserved by the WCN schemes. The non-flat bottom is given by

$$b(x,y)=0.8e^{-50((x-0.5)^2+(y-0.5)^2)}. \tag{4.10}$$

https://doi.org/10.4208/cicp.OA-2016-0200 Published online by Cambridge University Press

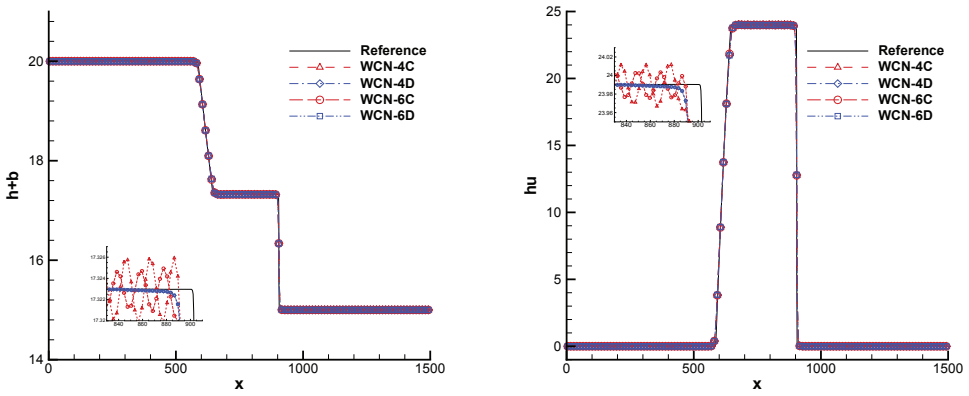


Figure 5: One-dimensional dam-breaking problem. (Left) The water surface level $h+b$ and (Right) the water discharge hu as computed by the WCN schemes at time $t=15$.

The initial conditions are

$$h(x,y,0)=1-b(x,y),\quad u(x,y,0)=v(x,y,0)=0. \tag{4.11}$$

The computational domain is $[0,1]\times[0,1]$ and the final time is $t=0.1$. The stationary solution should be exactly maintained by the theoretical analysis.

The double precision is used again to perform the computation. The L_∞ errors in the water surface level $h+b$ and water discharges hu and hv as computed by the WCN schemes at the final time is shown in Table 4 which are at the level of round-off errors for different resolutions with $N\times M=100\times100$, 200×200, 400×400. Obviously, the exact C-property is preserved.

Table 4: The two-dimensional exact C-property test. L_∞ errors in the water surface level $h+b$ and water discharges hu and hv as computed by the WCN schemes with the smooth bottom topographies $b(x,y)$.

N	100×100			200×200			400×400		
L_∞	$h+b$	hu	hv	$h+b$	hu	hv	$h+b$	hu	hv
WCN-4C	6.7E-16	2.2E-15	2.0E-15	8.9E-16	3.3E-15	3.4E-15	1.2E-15	7.1E-15	7.4E-15
WCN-6C	6.7E-16	2.1E-15	2.3E-15	8.9E-16	3.5E-15	3.4E-15	1.1E-15	7.2E-15	6.6E-15
WCN-4D	6.7E-16	2.2E-15	2.1E-15	8.9E-16	4.0E-15	3.5E-15	1.1E-15	6.0E-15	5.7E-15
WCN-6D	6.7E-16	2.0E-15	2.0E-15	8.9E-16	3.7E-15	3.6E-15	1.1E-15	5.8E-15	5.7E-15

4.7 A small perturbation of two-dimensional steady-state water

This is a classical two-dimensional example in the literature [19] to demonstrate the capability of the proposed scheme for a perturbation of a stationary state. An isolated elliptical

https://doi.org/10.4208/cicp.OA-2016-0200 Published online by Cambridge University Press

shaped bottom topography is defined by

$$b(x,y)=0.8e^{-5(x-0.9)^2-50(y-0.5)^2}. \tag{4.12}$$

The initial conditions are

$$h(x,y,0)=\begin{cases} 1-b(x,y)+0.01, & \text{if} \quad 0.05\le x\le 0.15, \\ 1-b(x,y), & \text{otherwise}, \end{cases} \qquad u(x,y,0)=v(x,y,0)=0. \tag{4.13}$$

The computational domain is $[0,2]\times[0,1]$ and the final time is $t=0.6$.

We present the water surface level $h+b$ as computed by the WCN schemes with resolution 600×300 at times $t=0.12$, 0.24, 0.36, 0.48 and 0.60 in Fig. 6 and Fig. 7 respectively.

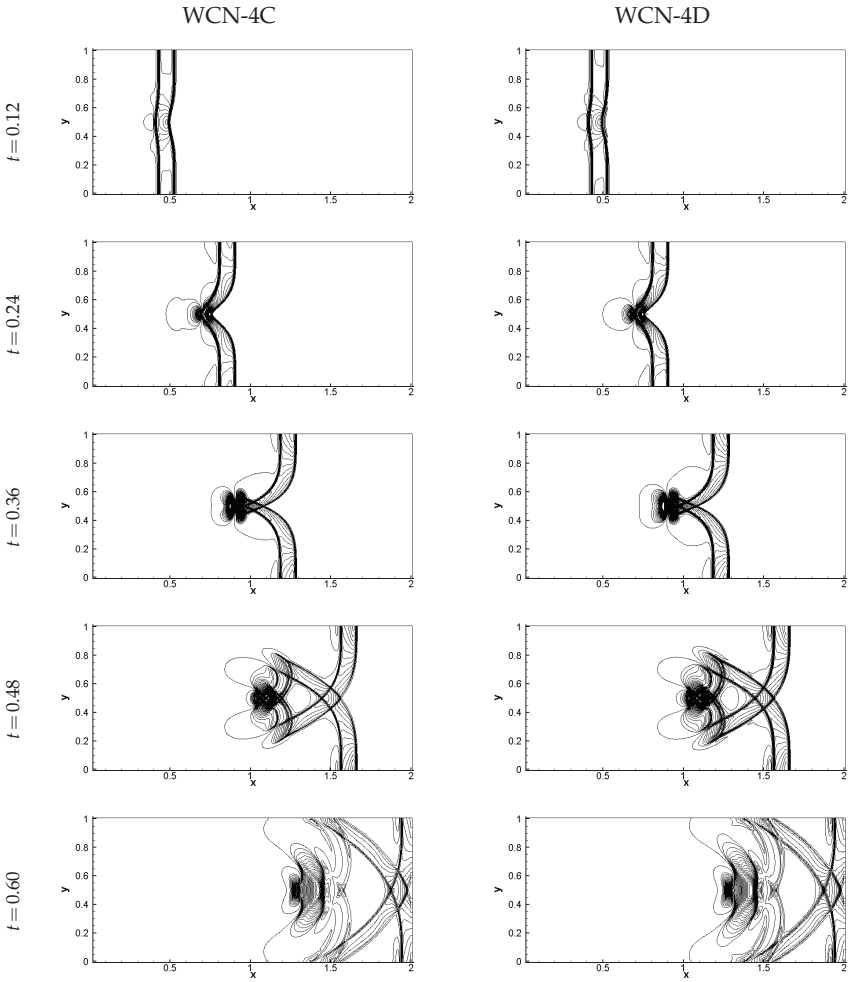


Figure 6: A small perturbation of two-dimensional steady state water. The water surface level $h+b$ as computed by (Left) the WCN-4C scheme and (Right) the WCN-4D scheme at times $t=0.12$, 0.24, 0.36, 0.48 and 0.60.

https://doi.org/10.4208/cicp.OA-2016-0200 Published online by Cambridge University Press

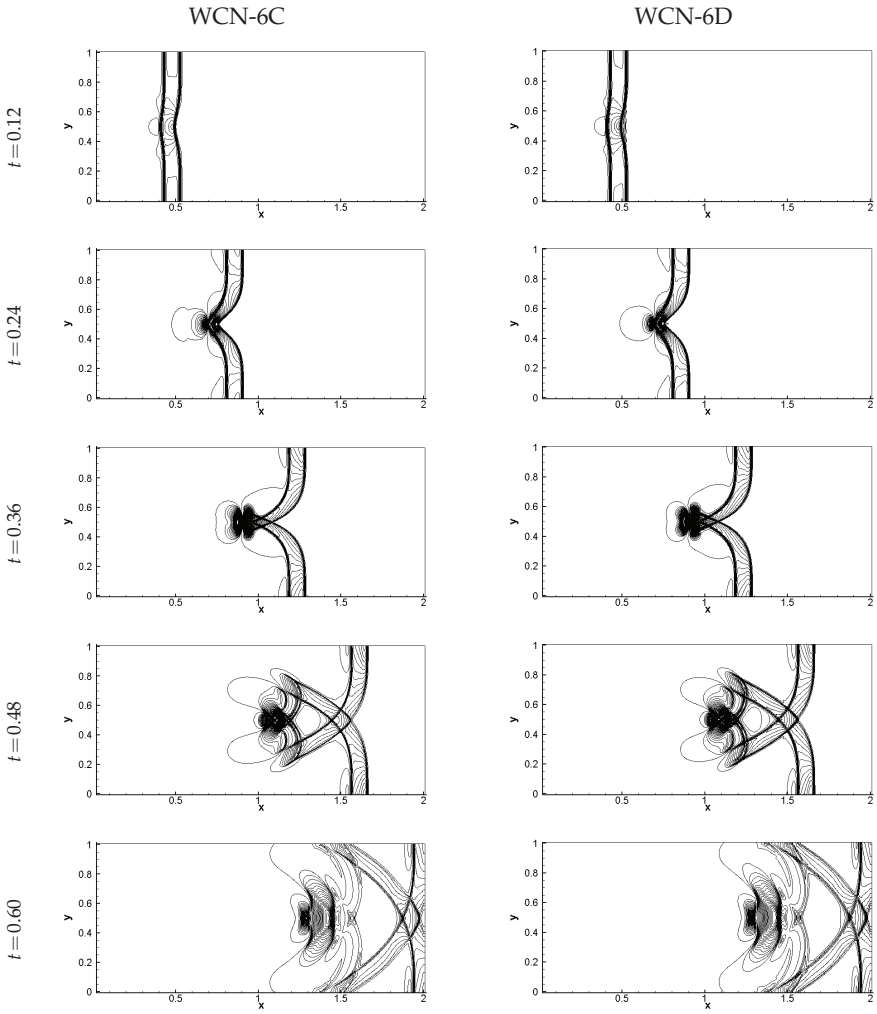


Figure 7: A small perturbation of two-dimensional steady state water. The water surface level $h+b$ as computed by (Left) the WCN-6C scheme and (Right) the WCN-6D scheme at times $t=0.12$, 0.24, 0.36, 0.48 and 0.60.

The results reach a good agreement with those in the literature [19, 21, 34]. From the figures, the right-going disturbance propagating past the hump can be clearly observed. The complex and small scale structures of the flow are resolved very well by the WCN schemes.

5 Concluding remarks

In this paper we extend the high order weighted compact nonlinear (WCN) schemes to solve the one- and two-dimensional shallow water equations. The fifth-order up-

https://doi.org/10.4208/cicp.OA-2016-0200 Published online by Cambridge University Press

wind weighted nonlinear interpolations are combined with the fourth/sixth order cell-centered compact schemes with/without local characteristic projections to construct the WCN schemes. A special splitting technique of the source terms allows us to design specific approximations such that the resulting WCN schemes satisfy the exact C-property for the still water stationary solutions, and at the same time maintain their original high order accuracy and essentially nonoscillatory property for the general solutions. Moreover, the proposed schemes can be proved to exactly maintain the steady state solution by the rigorous theoretical analysis. We use the first order global Lax-Friedrichs flux splitting to introduce correct upwinding and enhance the numerical stability. The extensive numerical results show that the proposed schemes maintain the exact C-property, accuracy, and nonoscillatory shock capturing. Furthermore, we observe that the WCN schemes without local characteristic projections usually generate more numerical oscillations around the discontinuities and high gradients than those with local characteristic projections.

In our future work in this area, we will explore the well-balanced WCN scheme based on the variable interpolation [9] for the shallow water equations in detail and show the comparative results with this work in the near future.

Acknowledgments

The authors would like to express our sincere gratitude to anonymous reviewers and Prof. Yulong Xing for their valuable suggestions on improving the quality of this work. The authors would like to acknowledge the funding support of this research by National Natural Science Foundation of China (11201441, 41306002) and Fundamental Research Funds for the Central Universities (201562012, 201564019). The first author gratefully acknowledges the invitation of Dr. G.H. Hu and also extends his gratitude to the Faculty of Science and Technology at University of Macau for hosting his visit. The work of G. H. Hu was partially supported by 050/2014/A1 from FDCT of Macao S.A.R., MYRG2014-00109-FST from University of Macau, and National Natural Science Foundation of China (Grant No. 11401608).

References

[1] F. Alcrudo and F. Benkhaldoun, Exact solutions to the Riemann problem of the shallow water equations with a bottom step, Comput. Fluids. 30 (2001) 643–671.
[2] A. Bermudez and M.E. Vazquez, Upwind methods for hyperbolic conservation laws with source terms, Comput. Fluids. 23 (1994) 1049–1071.
[3] R. Borges, M. Carmona, B. Costa and W.S. Don, An improved weighted essentially non-oscillatory scheme for hyperbolic conservation laws, J. Comput. Phys. 227 (2008) 3101–3211.
[4] M. Castro, B. Costa and W.S. Don, High order weighted essentially non-oscillatory WENO-Z schemes for hyperbolic conservation laws, J. Comput. Phys. 230 (2011) 1766–1792.

https://doi.org/10.4208/cicp.OA-2016-0200 Published online by Cambridge University Press

[5] N. Crnjaric-Zic, S. Vukovic and L. Sopta, Extension of ENO and WENO schemes to one-dimensional sediment transport equations, Comput. Fluids 33 (2004) 31–56.
[6] J. Deng, R. Li, T. Sun and S. Wu, Robust a simulation for shallow flows with friction on rough topography, Numer. Math. Theor. Meth. Appl. 6 (2013) 384–407.
[7] X. Deng, M. Mao, Y. Jiang and H. liu, New high-order hybrid cell-edge and cell-node weighted compact nonlinear scheme. In: Proceedings of 20th AIAA CFD conference, AIAA 2011-3847, June 27-30, Honoluu, HI, USA, 2011.
[8] X. Deng and H. Maekawa, Compact high-order accurate nonlinear schemes, J. Comput. Phys. 130 (1997) 77–91.
[9] X. Deng and H. Zhang, Developing high-order weighted compact nonlinear schemes, J. Comput. Phys. 165 (2000) 22–44.
[10] W.S. Don, Z. Gao, P. Li and X. Wen, Hybrid Compact-WENO Finite Difference Scheme with Conjugate Fourier Shock Detection Algorithm for Hyperbolic Conservation Laws, SIAM, J. Sci. Comput. 38(2) (2016) A691–A711.
[11] A. Ern, S. Piperno and K. Djadel, A well-balanced Runge-Kutta discontinuous Galerkin method for the shallow-water equations with flooding and drying, Int. J. Numer. Methods Fluids 58 (2008) 1–25.
[12] R. Gandham and D. Medina and T. Warburton, GPU Accelerated Discontinuous Galerkin Methods for Shallow Water Equations, Commun. Comput. Phys. 18 (2015) 37–64.
[13] R. Iida, M. Asahara, A.K. Hayashi, N. Tsuboi and T. Nonomura, Implementation of a Robust Weighted Compact Nonlinear Scheme for Modeling of Hydrogen/Air Detonation, Combut. Sci. Tech. 186 (2014) 1736–1757.
[14] G.S. Jiang and C.-W. Shu, Efficient Implementation of Weighted ENO Schemes, J. Comput. Phys. 126 (1996) 202–228.
[15] E. Johnsen, J. Larsson, A.V. Bhagatwala, W.H. Cabot, P. Moin, B.J. Olson, et al. Assessment of high-resolution methods for numerical simulations of compressible turbulence with shock waves, J. Comput. Phys. 229(4) (2010) 1213–37.
[16] D.Y. Kuang and L. Lee, A conservative formulation and a numerical algorithm for the double-gyre nonlinear shallow-water model, Numer. Math. Theor. Meth. Appl. 8 (2015) 634–650.
[17] Y.Y. Kuang, K.L. Wu and H.Z. Tang, Runge-Kutta discontinuous local evolution Galerkin methods for the shallow water equations on the cubed-sphere grid, Numer. Math. Theor. Meth. Appl. 10 (2017) 373–419.
[18] S.A. Lele, Compact finite difference schemes with spectral-like resolution, J. Comput. Phys. 103(1) (1992) 16–42.
[19] R.J. LeVeque, Balancing source terms and flux gradients on high-resolution Godunov methods: the quasi-steady wave propagation algorithm, J. Comput. Phys. 146 (1998) 346–365.
[20] X.L. Liu, S.H. Zhang, H.X. Zhang and C.-W. Shu, A new class of central compact schemes with spectral-like resolution I: Linear schemes, J. Comput. Phys. 248 (2013) 235–256.
[21] G. Li, C.N. Lu and J.X. Qiu, Hybrid well-balanced WENO schemes with different indicators for shallow water equations, J. Sci. Comput. 51 (2012) 527–559.
[22] T. Nonomura and K. Fujii, Effects of difference scheme type in high-order weighted compact nonlinear schemes, J. Comput. Phys. 228 (2009) 3533–3539.
[23] T. Nonomura and K. Fujii, Robust explicit formulation of weighted compact nonlinear scheme, Comput. Fluids 85 (2013) 8–18.
[24] T. Nonomura, N. Iizuka and K. Fujii, Freestream and vortex preservation properties of high-order WENO and WCNS on curvilinear grids, Comput. Fluids 39(2) (2010) 197–214.

https://doi.org/10.4208/cicp.OA-2016-0200 Published online by Cambridge University Press

[25] T. Nonomura, N. Iizuka and K. Fujii, Increasing order of accuracy of weighted compact nonlinear scheme, In: AIAA-2007-893, 2007.
[26] Y.X. Ren, M. Liu and H. Zhang, A characteristic-wise hybrid compact-WENO scheme for solving hyperbolic conservation laws, J. Comput. Phys. 192 (2003) 365–386.
[27] B.D. Rogers, A.G.L. Borthwick and P.H. Taylor, Mathematical balancing of flux gradient and source terms prior to using Roes approximate Riemann solver, J. Comput. Phys. 192 (2003) 422–451.
[28] C.-W. Shu, Essentially non-oscillatory and weighted essentially non-oscillatory schemes for hyperbolic conservation laws, in: B. Cockburn, C. Johnson, C.-W. Shu, E. Tadmor (Ed.: A. Quarteroni) Advanced Numerical Approximation of Nonlinear Hyperbolic Equations, Lecture Notes in Mathematics, vol. 1697, Springer, 1998, pp. 325–432.
[29] C.-W. Shu and S. Osher, Efficient implementation of essentially non-oscillatory shock-capturing schemes, J. Comput. Phys. 77 (1988) 439–471.
[30] G. Stecca, A. Siviglia and E. F. Toro, A Finite Volume Upwind-Biased Centred Scheme for Hyperbolic Systems of Conservation Laws: Application to Shallow Water Equations, Commun. Comput. Phys. 12 (2012) 1183-1214.
[31] S. Vukovic, N. Crnjaric-Zic and L. Sopta, WENO schemes for balance laws with spatially varying flux, J. Comput. Phys. 199 (2004) 87–109.
[32] S. Vukovic and L. Sopta, ENO and WENO schemes with the exact conservation property for one-dimensional shallow water equations, J. Comput. Phys. 179 (2002) 593–621.
[33] Y. Xing and C.-W. Shu, A survey of high order schemes for the shallow water equations, J. Math. Study 47 (2014) 221–249.
[34] Y. Xing and C.-W. Shu, High order finite difference WENO schemes with the exact conservation property for the shallow water equations, J. Comput. Phys. 208 (2005) 206–227.
[35] Y. Xing and X. Zhang, Positivity-preserving well-balanced discontinuous Galerkin methods for the shallow water equations on unstructured triangular meshes, J. Sci. Comput. 57 (2013) 19–41.
[36] Y. Xing, X. Zhang and C.-W. Shu, Positivity-preserving high order well-balanced discontinuous Galerkin methods for the shallow water equations, Adv. Water Resour. 33 (2010) 1476–1493.
[37] S. Zhang, S. Jiang and C.-W. Shu, Development of nonlinear weighted compact schemes with increasingly higher order accuracy, J. Comput. Phys. 227 (2008) 7294–321.
[38] J.G. Zhou, D.M. Causon, C.G. Mingham and D.M. Ingram, The surface gradient method for the treatment of source terms in the shallow-water equations, J. Comput. Phys. 168 (2001) 1–25.
[39] Q.Q. Zhu, Z. Gao, W.S. Don and X.Q. Lv, Well-balanced Hybrid Compact-WENO Schemes for Shallow Water Equations, Appl. Num. Math. 112 (2017) 65–78.

https://doi.org/10.4208/cicp.OA-2016-0200 Published online by Cambridge University Press